Ocean Engineering 38 (2011) 1237–1245

Contents lists available at ScienceDirect

Ocean Engineering

journal homepage: www.elsevier.com/locate/oceaneng

Wave interaction with a wave absorbing double curtain-wall breakwater

Yong Liu [a,*], Yu-cheng Li [b]

[a] College of Engineering, Ocean University of China, Qingdao 266100, China
[b] State Key Laboratory of Coastal and Offshore Engineering, Dalian University of Technology, Dalian 116024, China

ARTICLE INFO

Article history:
Received 22 September 2009
Accepted 15 May 2011
Editor-in-Chief: A.I. Incecik
Available online 8 June 2011

Keywords:
Curtain-wall breakwater
Perforated wall
Reflection coefficient
Transmission coefficient
Wave force

ABSTRACT

This study examines the hydrodynamic performance of a wave absorbing double curtain-wall breakwater. The breakwater consists of a seaward perforated wall and a shoreward impermeable wall. Both walls extend from above the seawater to some distance above the seabed. Then the below gap allows the seawater exchange, the sediment transport and the fish passage. By means of the eigenfunction expansion method and a least square approach, a linear analytical solution is developed for the interaction of water waves with the breakwater. Then the reflection coefficient, the transmission coefficient and the wave forces acting on the walls are calculated. The numerical results obtained for limiting cases agree very well with previous predictions for a single partially immersed impermeable wall, the double partially immersed impermeable walls and the bottom-standing Jarlan-type breakwater. The predicted reflection coefficients for the present breakwater also agree reasonable with previous experimental results. Numerical results show that with appropriate structure parameters, the reflection and transmission coefficients of the breakwater may be both below 0.5 at a wide range of the relative water depth. At the same time, the magnitude of wave force acting on each wall is small. This is significant for practical engineering.

1. Introduction

Recently, both wave absorbing Jarlan-type perforated-wall breakwaters and partially immersed vertical walls (curtain-wall breakwaters) have been often used to protect harbor and coastline due to their intrinsic merits. The original Jarlan-type perforated breakwater (Jarlan, 1961) consists of a perforated front wall, an impermeable rear wall and a wave-absorbing chamber between them. It can effectively reduce the wave forces acting on, the wave reflection from and the wave run-up in front of the structure (Suh et al., 2006a; Li, 2007). The smaller wave force is significant to ensure the stability of the breakwater. The lower reflection benefits a lot to the safe navigation of vessels near the structure. It is also helpful to reducing the scour of seabed in front of the breakwater. But the conventional Jarlan-type structure is bottom-standing and thus the free exchange of seawater between shelter and open regions fails. The vertical wall extending from above the seawater to some distance above the seabed may be used as an alternative. Then the gap between the wall tip and the seabed allows the water circulation, the sediment transport and the fish passage, which prevents the deterioration of coastal marine environment. The partially immersed walls are also less dependent on local seabed geological conditions. Moreover, the partially immersed structure can provide more economical shelter in deeper water as the wave energy mainly concentrates near the free surface (Isaacson et al., 1998; Rageh et al., 2009).

It is natural to combine the above two types of breakwaters by considering their merits. This leads to the so called partially immersed wave absorbing perforated breakwater (or wave absorbing curtain-wall breakwater). This paper aims to develop an effective analytical solution for the interaction of water waves with the partially immersed wave absorbing perforated breakwater and then give more understanding on the breakwater's hydrodynamic performance. Hence previous studies on conventional Jarlan-type breakwaters and partially immersed vertical walls are both reviewed.

Since the initial study of Jarlan (1961), the interactions of water waves with Jarlan-type structures have been studied many times by different researchers. Most of these studies have focused on the reflection coefficient of single perforated wall structures (e.g., Tanimoto and Yoshimoto, 1982; Chwang and Dong, 1984; Bennett et al., 1992; Sahoo et al., 2000; Zhu and Chwang, 2001; Li et al., 2002; Suh et al., 2006a; Ketabdari and Varjavand, 2008). These studies have shown that the reflection coefficient is mainly determined by the front wall porosity and the ratio of the wave chamber width to the incident wavelength. By means of suitable design, the reflection coefficient can attain a very small value. In order to further enhance the breakwater's wave absorbing ability, structures with two or multiple perforated front walls have also been proposed and studied (e.g., Twu and Lin, 1991; Fugazza and Natale, 1992; Williams et al., 2000; Huang, 2006).

* Corresponding author. Tel.: +86 532 66781129; fax: +86 532 66781550.
E-mail addresses: liuyong_77@hotmail.com (Y. Liu), liyuch@dlut.edu.cn (Y.-c. Li).

0029-8018/$ - see front matter © 2011 Elsevier Ltd. All rights reserved.
doi:10.1016/j.oceaneng.2011.05.009

At this time, the geometrical porosities of the front walls should be designed in a gradually decreasing order along the incident wave propagation direction (Twu and Lin, 1991). Besides the reflection coefficient, the stability of the perforated breakwater has also been examined in the past. According to experimental results, Takahashi (1996), Tabet-Aoul and Lambert (2003), Li (2007) and Chen et al. (2009) have developed different empirical methods to estimate the wave forces acting on perforated caissons. These methods may be used for practical designs. By means of matched eigenfunction expansion method, several researchers (Yip and Chwang, 2000; Teng et al., 2004; Liu et al., 2007) examined analytically the horizontal wave forces acting on perforated breakwaters. More recently, Liu et al. (2008) examined both horizontal and vertical forces acting on perforated caissons by using the eigenfunction expansion method and the finite element method. It is noted that the aforementioned Jarlan-type structures are all bottom-standing.

The earlier studies on wave interaction with a single partially immersed impermeable wall can be found in Ursell (1947) and Wiegel (1960). Ursell (1947) used modified Bessel function to calculate the transmission coefficient of the vertical thin wall in deepwater. Wiegel (1960) used the power transmission theory to give an approximate solution to the reflection and transmission coefficients of the wall. The method of Wiegel (1960) has also been further developed by Kriebel and Bollmann (1996). More studies on this topic have been carried out by means of the eigenfunction expansion method (Losada et al., 1992; Abul-Azm, 1993; Suh et al., 2006b), the multi-term Galerkin method (Porter and Evans, 1995), physical model tests (Reddy and Neelamani, 1992) and different boundary element methods (Liu and Abbaspour, 1982; Chen et al., 2004). These studies indicated that the partially immersed wall with adequate draft can effectively reduce the height of transmitted wave in deeper water. To further reduce the height of transmitted wave, double or more partially immersed impermeable walls have been proposed and studied (e.g., McIver, 1985; Das et al., 1997; Neelamani and Vedagiri, 2002; Lee and Lo, 2002; Günaydın and Kabdaşlı, 2007). With suitable separation between two walls, the double walls can provide more effective shelter in comparison with the single wall. But at some special conditions, a full transmission may occur in theory (McIver, 1985; Das et al., 1997). This must be excluded in practical designs. For above impermeable walls, the horizontal wave forces acting on the structure may comparatively large. This is rather disadvantage for the stability of pile-supported structures. Then the perforated wall can be used as an alternative. The correlative studies can be found in Isaacson et al. (1998, 1999), Lee and Chwang (2000) and Huang (2007).

As mentioned at beginning, the combination of the partially immersed wall and the wave absorbing Jarlan-type breakwater leads to the partially immersed wave absorbing breakwater, which has more merits. Cox et al. (1998) and Brossard et al. (2003) have carried out experimental studies on the hydrodynamic performance of partially immersed wave absorbing breakwaters. The breakwater examined by Cox et al. (1998) mainly consisted of a seaward vertical perforated wall and a shoreward vertical impermeable wall. The two walls supported on piles were connected by a top deck for pedestrian. This structure was proposed to alter the old breakwater for a yacht club in Sydney's north, where the reflection and transmission coefficients were both required to be below 30% (the mean water depth and the wave period are 10 m and 2.8 s, respectively). With suitable design, very small reflection and transmission coefficients were simultaneously obtained by Cox et al. (1998). Differing from Cox et al. (1998), Brossard et al. (2003) proposed and studied a partially immersed rectangular caisson with a perforated front wall. They found that when the draft was half of the water depth, the minimum reflection coefficient of the perforated structure was about 5%, and that the corresponding transmission coefficient was about 20–30%. Since the partially immersed wave absorbing structure is so effective, more relevant studies should be carried out. Especially, the analytical solution may give more scientific insight on the hydrodynamic performance of the structure. But this has been scarcely referred so far. Therefore, this study will develop an analytical solution for the interaction of water waves with the partially immersed wave absorbing breakwater and then carefully examine the structure's hydrodynamic performance by numerical results. At the present stage, the simplest configuration consisting of a perforated front wall and an impermeable rear wall is considered.

In the following section, the boundary value problem for the interaction of water waves with the breakwater is formulated on the basis of the linear potential theory. In Section 3, an analytical solution to the boundary value problem is developed. The whole fluid domain is divided into three regions according to the division of the structure, and the eigenfunction expansion method is used to obtain the velocity potential in each domain. Then a least square approach is adopted to determine the unknown expansion coefficients in velocity potentials. Subsequently, the reflection and transmission coefficients and the wave forces acting on the walls are obtained. In Section 4, the new developed solution are validated by comparing predicted results with previous numerical results of Porter and Evans (1995), Das et al. (1997) and Sahoo et al. (2000), as well as previous experimental results of Cox et al. (1998). Numerical examples are also presented to examine the hydrodynamic performance of the breakwater. Some useful results are presented for practical engineering. Finally, the main conclusions of this study are drawn.

2. Mathematical formulation

The idealized geometry of the two-dimensional problem is shown in Fig. 1. A double curtain-wall breakwater consisting of a seaward perforated wall and a shoreward impermeable wall is partially immersed in a water channel of constant depth h. The draft of the breakwater is d. The width of the wave-absorbing chamber (the separation between front and rear walls) is B, and equals $2b$. The perforated breakwater is subject to normally incident regular waves of height H and wavelength L. A Cartesian coordinate system (x, z) is defined with the origin at the intersection of the still water level and the wave chamber midline, the z-axis in the vertical direction upward and the x-axis in the direction of incident wave propagation. The whole fluid domain is divided into three regions: region 1, the fluid domain at the left-hand side of the front wall; region 2, the fluid domain between the two walls; and region 3, the fluid domain at the right-hand side of the rear wall. In the present study, the thickness of each wall is assumed to be zero, as they are very small compared with the incident wavelength.

It is assumed that the fluid is inviscid and incompressible, the fluid motion is irrotational and that the incident wave is of small

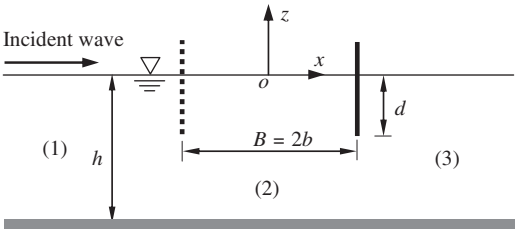

Fig. 1. The coordinate system and main structure.

amplitude. Then a velocity potential $\Phi(x,z,t)$ can be used to describe the fluid motion. For monochromatic incident waves with angular frequency ω, the time factor $e^{-i\omega t}$ can be separated and thus the velocity potential and the dynamic water pressure can be written as

$$\Phi(x,z,t) = \mathrm{Re}[\phi(x,z)e^{-i\omega t}], \tag{1}$$

$$P(x,z,t) = \mathrm{Re}[p(x,z)e^{-i\omega t}], \tag{2}$$

where Re[ ] denotes the real part of the argument; $i=\sqrt{-1}$; t is time; and ϕ and p denote the spatial velocity potential and the dynamic pressure, respectively.

In different regions, the spatial potentials all satisfy the Laplace equation

$$\frac{\partial^2\phi_j(x,z)}{\partial x^2}+\frac{\partial^2\phi_j(x,z)}{\partial z^2}=0 \quad j=1,2,3, \tag{3}$$

where the subscript j represents variables with respect to the region j.

These potentials are also required to satisfy appropriate boundary conditions on the free surface, seabed surface and far field:

$$\frac{\partial\phi_j}{\partial z}=\frac{\omega^2}{g}\phi_j, \quad z=0, \quad j=1,2,3, \tag{4}$$

$$\frac{\partial\phi_j}{\partial z}=0, \quad z=-h, \quad j=1,2,3, \tag{5}$$

$$\lim_{x\to+\infty}\left(\frac{\partial\phi_3}{\partial x}-ik_0\phi_3\right)=0, \tag{6a}$$

$$\lim_{x\to-\infty}\left(\frac{\partial\phi_R}{\partial x}+ik_0\phi_R\right)=0, \tag{6b}$$

where g is gravitational acceleration; k_0 is the incident wave number; and ϕ_R is the velocity potential of reflected waves.

Furthermore, the velocity potentials must satisfy the matching boundary conditions at the interfaces, $x=-b$ and b

$$\frac{\partial\phi_1}{\partial x}=\frac{\partial\phi_2}{\partial x}=ik_0G(\phi_1-\phi_2), \quad x=-b, \quad -d\le z\le 0, \tag{7}$$

$$\frac{\partial\phi_1}{\partial x}=\frac{\partial\phi_2}{\partial x}, \quad x=-b, \quad -h\le z\le -d, \tag{8}$$

$$\phi_1=\phi_2, \quad x=-b, \quad -h\le z\le -d, \tag{9}$$

$$\frac{\partial\phi_2}{\partial x}=\frac{\partial\phi_3}{\partial x}=0, \quad x=b, \quad -d\le z\le 0, \tag{10}$$

$$\frac{\partial\phi_2}{\partial x}=\frac{\partial\phi_3}{\partial x}, \quad x=b, \quad -h\le z\le -d, \tag{11}$$

$$\phi_2=\phi_3, \quad x=b, \quad -h\le z\le -d, \tag{12}$$

where G is the dimensionless porous effect parameter of a thin perforated wall (Chwang, 1983; Yu, 1995). Here the perforated wall is treated as the rigid homogeneous porous medium. The porous medium has three intrinsic parameters of the geometrical porosity ε, the linearized resistance coefficient f and the inertial effect coefficient s (Sollitt and Cross, 1972). Then following Yu (1995), the porous effect parameter G can be expressed as

$$G=\frac{\varepsilon}{k_0\delta(f-is)}=|G|e^{i\theta}, \quad 0\le\theta\le\pi/2, \tag{13}$$

where, δ is the wall thickness and θ is the argument of the complex G. It is noted that when waves pass through a thin perforated wall, the wave energy dissipation and the phase shift of wave motion may both occur. The energy dissipation due to the resistance effect of the wall is relevant to the real part of G. But the phase shift due to the inertial effect of the wall is relevant to the imaginary part of G. When $|G|$ equals zero, the perforated wall reduces to an impermeable wall, while for $|G|$ tends toward infinity, the wall becomes entirely transparent. It is also noted that when considering wave diffraction by the whole structure, the plate thickness is assumed to be zero. But the wall thickness should be considered when calculating G.

It should be mentioned that Eqs. (8) and (11) denote the horizontal mass fluxes must be continuous at interfaces. Eqs. (9) and (12) denote the dynamic pressures must be continuous at interfaces. Eq. (7) is the porous boundary conditions (Yu, 1995). The first equal sign in Eq. (7) denotes that the horizontal mass fluxes between regions 1 and 2 must be continuous at the seaward perforated wall. The second equal sign denotes that the normal fluid velocity passing through a thin perforated wall is linearly proportional to the pressure difference between the two sides of the wall under the linear assumption (Chwang, 1983).

3. Analytical solutions

By the separation of variables, the velocity potentials that satisfy Eq. (3) and the relevant boundary conditions, Eqs. (4)–(6a), (6b), can be written as

$$\phi_1=-\frac{igH}{2\omega}\left[e^{-\alpha_0(x+b)}Z_0(z)+R_0e^{\alpha_0(x+b)}Z_0(z)+\sum_{n=1}^{\infty}R_ne^{\alpha_n(x+b)}Z_n(z)\right], \tag{14}$$

$$\phi_2=-\frac{igH}{2\omega}\left[\sum_{n=0}^{\infty}A_ne^{-\alpha_n(x+b)}Z_n(z)+\sum_{n=0}^{\infty}C_ne^{\alpha_n(x-b)}Z_n(z)\right], \tag{15}$$

$$\phi_3=-\frac{igH}{2\omega}\left[T_0e^{-\alpha_0(x-b)}Z_0(z)+\sum_{n=1}^{\infty}T_ne^{-\alpha_n(x-b)}Z_n(z)\right], \tag{16}$$

where, R_n, A_n, C_n and T_n (n=0, 1, 2, …) are the unknown expansion complex coefficients, and $\alpha_0=-ik_0$ and $\alpha_n=k_n$ (n=1, 2, …). The wave numbers k_0 and k_n are the positive real roots of the following dispersion relations:

$$\omega^2=gk_0\tanh k_0h=-gk_n\tan k_nh, \quad n=1,2,\ldots. \tag{17}$$

In Eqs. (14)–(16), the depth-dependent functions $Z_n(z)$ (n=0, 1, 2, …) are given by

$$Z_0(z)=\cosh k_0(z+h)/\cosh k_0h, \tag{18a}$$

$$Z_n(z)=\cos k_n(z+h)/\cos k_nh, \quad n=1,2,\ldots. \tag{18b}$$

Then applying the matching boundary conditions, Eqs. (7)–(12), the unknown expansion coefficients can be determined. For convenience, these matching boundary conditions are rewritten as

$$\frac{\partial\phi_1}{\partial x}=\frac{\partial\phi_2}{\partial x}, \quad x=-b, \tag{19}$$

$$\frac{\partial\phi_2}{\partial x}=ik_0G(\phi_1-\phi_2), \quad x=-b, \quad -d\le z\le 0, \tag{20a}$$

$$\phi_1=\phi_2, \ x=-b, \ -h\le z\le -d, \tag{20b}$$

$$\frac{\partial\phi_2}{\partial x}=\frac{\partial\phi_3}{\partial x}, \quad x=b, \tag{21}$$

$$\frac{\partial \phi_2}{\partial x}=0, \quad x=b, \quad -d\le z\le 0, \tag{22a}$$

$$\phi_2=\phi_3, \quad x=b, \quad -h\le z\le -d. \tag{22b}$$

Substituting the expressions for the velocity potentials, Eqs. (14) and (15), into the boundary condition, Eq. (19), yields

$$R_0=1-A_0+X_0C_0, \tag{23a}$$

$$R_n=-A_n+X_nC_n, \quad n=1,2,\ldots. \tag{23b}$$

where $X_n=e^{-2\alpha_n b}$ $(n=0,1,2,\ldots)$. Substituting Eqs. (14) and (15) into Eqs. (20a) and (20b), and using the relationship of Eq. (23) gives

$$2ik_0GZ_0(z)+\sum_{n=0}^{\infty}(-2ik_0G+\alpha_n)A_nZ_n(z)-\sum_{n=0}^{\infty}\alpha_nX_nC_nZ_n(z)=0, \quad -d\le z\le 0, \tag{24a}$$

$$2Z_0(z)-2\sum_{n=0}^{\infty}A_nZ_n(z)=0, \quad -h\le z\le -d. \tag{24b}$$

Here we use a least square method (Dalrymple and Martin, 1990) to determine the unknown coefficients in Eqs. (24a) and (24b). In fact, this method has been used by many researchers (e.g., Losada et al., 1992; Abul-Azm, 1993; Sahoo et al., 2000; Lee and Lo, 2002). Now we define a new function $S(z)$ as follows:

$$S(z)=2ik_0GZ_0(z)+\sum_{n=0}^{\infty}(-2ik_0G+\alpha_n)A_nZ_n(z)-\sum_{n=0}^{\infty}\alpha_nX_nC_nZ_n(z), \quad -d\le z\le 0, \tag{25a}$$

$$S(z)=2Z_0(z)-2\sum_{n=0}^{\infty}A_nZ_n(z), \quad -h\le z\le -d. \tag{25b}$$

To satisfy $S(z)=0$ for $-h\le z\le 0$, the least square method requires

$$\int_{-h}^{0}|S(z)|^2\mathrm{d}z=\text{minimum}. \tag{26}$$

Minimizing the above integral with respect to each of the A_m $(m=0, 1, 2, \ldots)$ leads to

$$\int_{-h}^{0}S^*(z)\frac{\partial S(z)}{\partial A_m}\mathrm{d}z=0, \quad m=0,1,2,\ldots, \tag{27}$$

where the superscript asterisk denotes the complex conjugate. Then integrating with respect to z in Eq. (27) and truncating after N terms, yields a set of linear equations

$$[a_{mn}]_{N\times N}\{A_n^*\}_N+[b_{mn}]_{N\times N}\{C_n^*\}_N=-\{c_m\}_N, \tag{28}$$

where

$$a_{mn}=(-2ik_0G+\alpha_m)(2ik_0G^*+\alpha_n^*)\int_{-d}^{0}Z_m(z)Z_n(z)\mathrm{d}z+4\int_{-h}^{-d}Z_m(z)Z_n(z)\mathrm{d}z, \tag{29a}$$

$$b_{mn}=(-2ik_0G+\alpha_m)(-\alpha_n^*X_n^*)\int_{-d}^{0}Z_m(z)Z_n(z)\mathrm{d}z, \tag{29b}$$

$$c_m=(-2ik_0G+\alpha_m)(-2ik_0G^*)\int_{-d}^{0}Z_m(z)Z_0(z)\mathrm{d}z-4\int_{-h}^{-d}Z_m(z)Z_0(z)\mathrm{d}z. \tag{29c}$$

Substituting the expressions for the velocity potentials, Eqs. (15) and (16), into the boundary condition, Eq. (21), gives

$$T_n=X_nA_n-C_n, \quad n=0,1,2,\ldots. \tag{30}$$

Substituting Eqs. (15) and (16) into Eqs. (22a) and (22b), and using the relationship of Eq. (30) yields

$$-\sum_{n=0}^{\infty}\alpha_nX_nA_nZ_n(z)+\sum_{n=0}^{\infty}\alpha_nC_nZ_n(z)=0, \quad -d\le z\le 0, \tag{31a}$$

$$2\sum_{n=0}^{\infty}C_nZ_n(z)=0, \quad -h\le z\le -d. \tag{31b}$$

Using the same method as for Eq. (25) gives another set of linear equations

$$[d_{mn}]_{N\times N}\{A_n^*\}_N+[e_{mn}]_{N\times N}\{C_n^*\}_N=0, \tag{32}$$

where

$$d_{mn}=-\alpha_m\alpha_n^*X_n^*\int_{-d}^{0}Z_m(z)Z_n(z)\mathrm{d}z, \tag{33a}$$

$$e_{mn}=\alpha_m\alpha_n^*\int_{-d}^{0}Z_m(z)Z_n(z)\mathrm{d}z+4\int_{-h}^{-d}Z_m(z)Z_n(z)\mathrm{d}z. \tag{33b}$$

Then the unknown coefficients A_n^* and C_n^* can be obtained by solving linear Eqs. (28) and (32). Subsequently, all the unknown expansion coefficients in the velocity potentials are determined.

It is noted that the first part at the right-hand side of Eq. (14) denotes incident waves propagating in the positive x-direction, and the second part denotes reflected waves from the breakwater and the third part denotes a series of evanescent modes decaying in the negative x-direction. In addition, the first part at the right of Eq. (16) denotes transmitted waves propagating in the positive x-direction, and the second part denotes a series of evanescent modes decaying in the positive x-direction. The real reflection coefficient C_R is defined as the ratio of the reflected wave height to the incident wave height

$$C_R=|R_0|. \tag{34}$$

The real transmission coefficients C_T are defined as the ratio of the transmitted wave height to the incident wave height

$$C_T=|T_0|. \tag{35}$$

The energy-loss coefficient C_L can be calculated by

$$C_L=1-C_R{}^2-C_T{}^2, \tag{36}$$

when $|G|$ tends toward infinity or equals zero, the energy-loss coefficient is zero.

The dynamic pressure $p(x, z)$ can be obtained according to the Bernoulli equation

$$p(x,z)=i\rho\omega\phi(x,z), \tag{37}$$

where ρ is the fluid density. Then the wave force acting on each wall can be obtained by integrating the dynamic pressure along the structure. The magnitude of the horizontal wave force on the unit width of the front wall, F_f, is given as

$$F_f=i\rho\omega\int_{-d}^{0}(\phi_1-\phi_2)|_{x=-b}\mathrm{d}z=\frac{\rho\omega}{k_0G}\int_{-d}^{0}\frac{\partial\phi_1}{\partial x}|_{x=-b}\mathrm{d}z=\frac{\rho gH}{2ik_0G}\left[(R_0-1)\frac{\sinh k_0h-\sinh(k_0h-k_0d)}{i\cosh k_0h}+\sum_{n=1}^{N}R_n\frac{\sin k_nh-\sin(k_nh-k_nd)}{\cos k_nh}\right]. \tag{38}$$

The magnitude of the horizontal wave force on the unit width of the rear wall, F_r, is given as

$$F_r=i\rho\omega\int_{-d}^{0}(\phi_2-\phi_3)|_{x=b}\mathrm{d}z$$

$$= \rho g H \left[C_0 \frac{\sinh k_0 h - \sinh(k_0 h - k_0 d)}{k_0 \cosh k_0 h} + \sum_{n=1}^{N} C_n \frac{\sin k_n h - \sin(k_n h - k_n d)}{k_n \cos k_n h} \right]. \tag{39}$$

The dimensionless wave forces C_{Ff} and C_{Fr} on the front and rear walls are defined, respectively, as

$$C_{Ff} = \frac{|F_f|}{\rho g H h}, \tag{40}$$

$$C_{Fr} = \frac{|F_r|}{\rho g H h}. \tag{41}$$

4. Results and discussion

For the present method, the truncated number N in Eqs. (28) and (32) must be carefully determined to ensure the convergence of the solution. Due to the strong singularity in the fluid velocity near the wall tips, the rate of convergence for the solution is not very fast. But it is found that $N=400$ is enough to ensure at least two-figure accuracy for different configurations of the breakwater. This is sufficiently accurate for engineering purposes. The corresponding matrix equation can also be solved rapidly by standard solvers of linear algebraic equations in a personal computer. Thus the value of $N=400$ was adopted in the present study.

4.1. Comparisons with existed limiting cases

The present method was validated by comparing the numerical results for limiting cases with the results of Porter and Evans (1995), Das et al. (1997) and Sahoo et al. (2000).

When $|G|$ tends toward infinity, the front wall vanishes. Then the present structure reduces to a single partially immersed impermeable wall, as studied by Porter and Evans (1995). Fig. 2 shows a comparison for the reflection and transmission coefficients between the present results and the results of Porter and Evans (1995) at $d/h=0.5$ and $G=$Infinity. It can be seen from this figure that the agreement between these two results is very good. When $|G|$ equals zero, the front wall becomes impermeable. Then the present breakwater reduces to double partially immersed impermeable walls, as studied by Das et al. (1997). Fig. 3 shows a comparison for the reflection coefficient between the present results and the results of Das et al. (1997) at $d/h=0.2$ and $B/h=0.6$. It is evident from Fig. 3 that the agreement between these two results is also very good. It should be mentioned that the results of Porter and Evans (1995) are extremely accurate due to the use of the multi-term Galerkin method. But the application of the Galerkin method to the present structure is not straightforward.

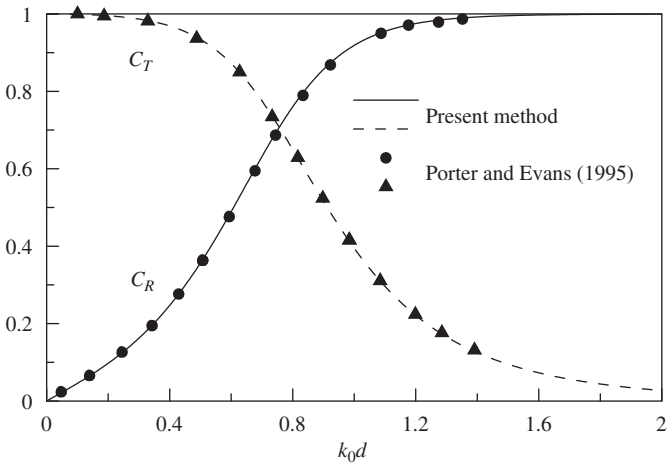

Fig. 2. Comparison between the present method and Porter and Evans (1995).

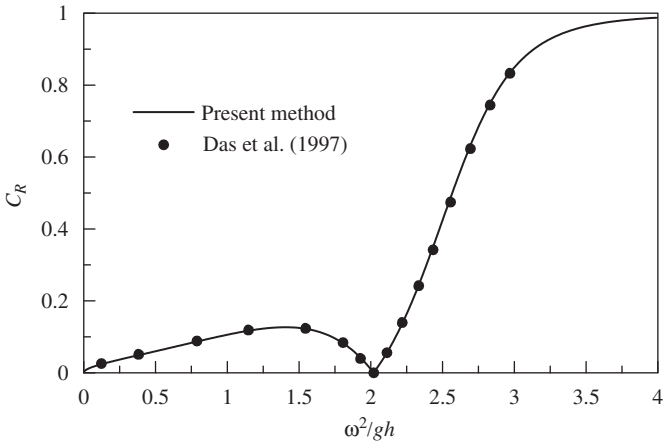

Fig. 3. Comparison between the present method and Das et al. (1997).

When the draft d equals the water depth h, the present structure becomes to the original bottom-standing Jarlan-type breakwater (Jarlan, 1961). At this time, the evanescent modes in the velocity potentials vanish, and the reflection coefficient can be calculated by (Sahoo et al., 2000)

$$C_R = \frac{1 - G(1 - i\cot k_0 B)}{1 + G(1 + i\cot k_0 B)}. \tag{42}$$

For $d=h$, the calculated reflection coefficients by the present method are exactly the same as that by Eq. (42). This is not plotted here for simplicity. In addition, the calculated transmission coefficients for $d=h$ always equal zero. This is physically natural.

4.2. Comparisons with experimental data

The present method was validated by comparing the numerical results of the reflection coefficient with the experimental data of Cox et al. (1998).

Cox et al. (1998) presented four groups of experimental data for the reflection coefficient in their paper. In their tests, the dimensionless incident wave number $k_0h=0.4\pi$, 0.6π and 0.8π, the geometrical porosity $\varepsilon=20\%$, and the relative draft $d/h=0.3$ and 0.5. These experimental data were all used to validate our present method. For calculating the reflection coefficient, the porous effect parameter G must be determined ahead by Eq. (13). The linearized resistance coefficient f in Eq. (13) was calculated by the following simple empirical formula (Li et al., 2006):

$$f = -3338.7(\delta/h)^2 + 82.769(\delta/h) + 8.711, \quad 0.0094 \le \delta/h \le 0.05. \tag{43}$$

The value of the dimensionless wall thickness δ/h was not given in Cox et al. (1998). A reasonable value of $\delta/h=0.02$ was adopted and thus $f=9.0$ by Eq. (43). The inertial coefficient s in Eq. (13) was treated as unity (Isaacson et al., 1998; Li et al., 2006).

The comparisons between our predictions and the experimental results of Cox et al. (1998) are shown in Fig. 4. In this figure, the circular dots represent the experimental results of Cox et al. (1998), whereas the lines are for our predictions. We note that due to a misprint in Cox et al. (1998), the data for the case of $k_0h=0.8\pi$ and $d/h=0.5$ was also denoted as the case of $k_0h=0.4\pi$ and $d/h=0.3$. This is excluded in our comparison.

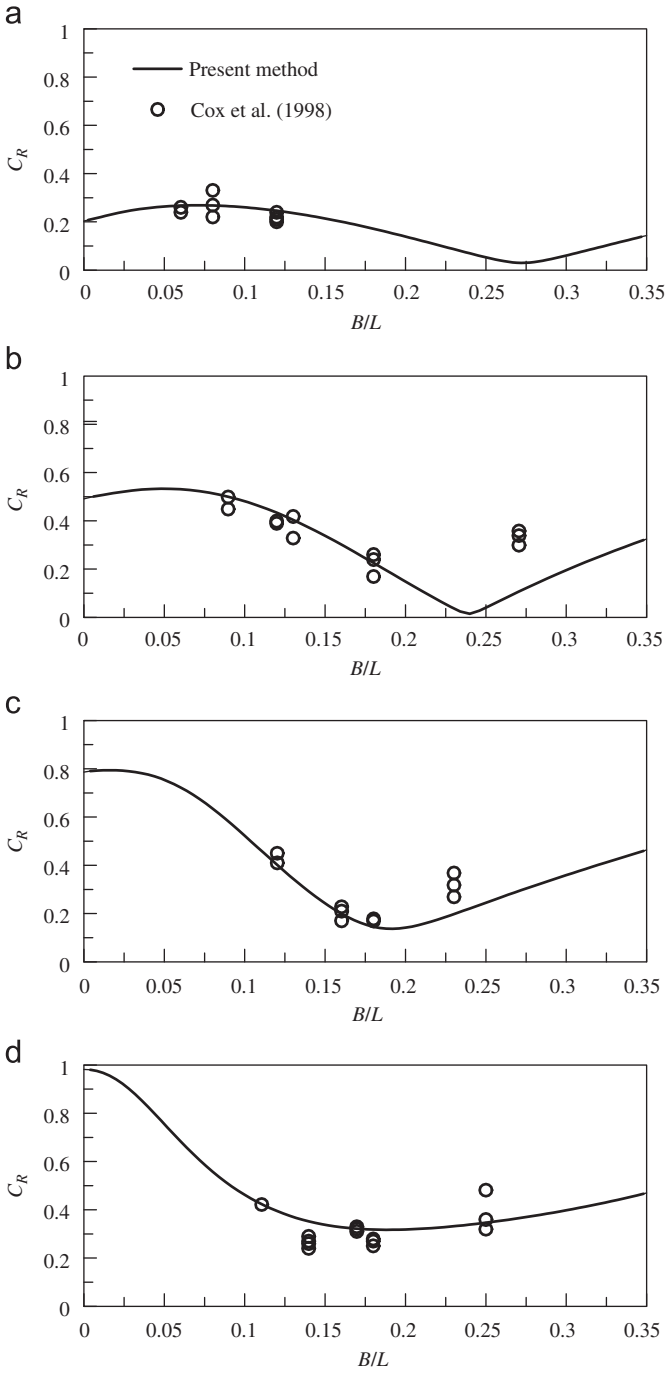

Fig. 4. Comparison between the present method and the experimental data of Cox et al. (1998): (a) $k_0h=0.4\pi$, $\varepsilon=20\%$, $d/h=0.3$; (b) $k_0h=0.6\pi$, $\varepsilon=20\%$, $d/h=0.3$; (c) $k_0h=0.8\pi$, $\varepsilon=20\%$, $d/h=0.3$; (d) $k_0h=0.8\pi$, $\varepsilon=20\%$, $d/h=0.5$.

It can be seen from Fig. 4 that the agreement between predictions and experimental results is reasonable. This indicates that with suitable porous effect parameter G, the present method should be effective for practical cases.

4.3. Numerical examples

The effects of the relative draft d/h of the breakwater on C_R and C_T are shown in Fig. 5 at $k_0h=1.6$ and $G=0.5e^{0i}=0.5$. In this figure, the reflection and transmission coefficients are plotted as the function of the relative wave chamber width B/L. Here the maximum value of B/L is 1.2 for illustration, although the practical

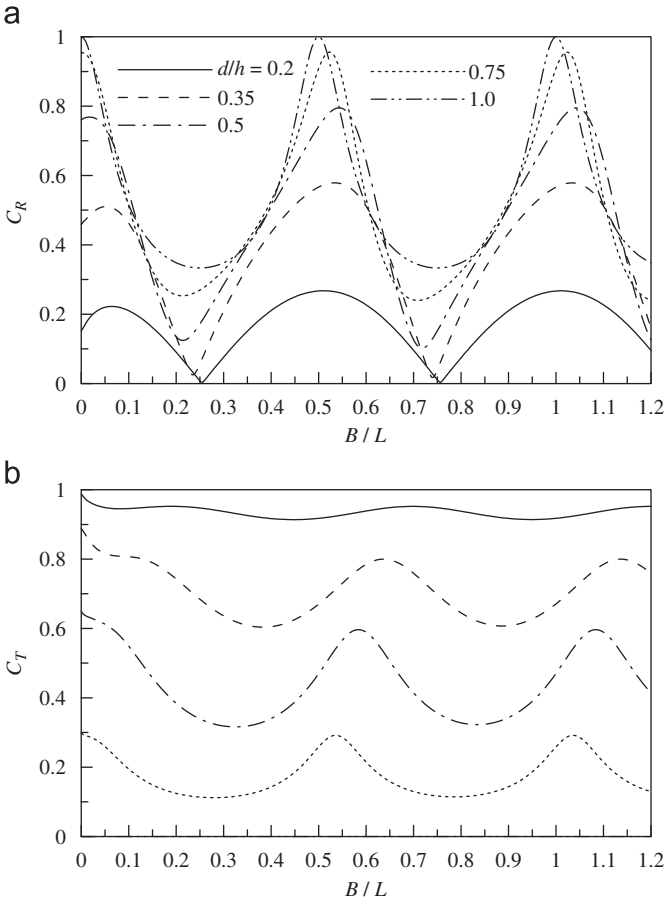

Fig. 5. Effects of d/h on C_R and C_T: $k_0h=1.6$ and $G=0.5e^{0i}$. (a) C_R; (b) C_T.

value of B/L is usually below 0.5. The double dot dash line in Fig. 5a denotes the original bottom-standing Jarlan-type perforated breakwater. This structure has been thoroughly studied by Chwang and Dong (1984), Fugazza and Natale (1992) and Sahoo et al. (2000). According to their studies, the reflection coefficient periodically reaches a minimum at $B/L=0.5n+0.25$ ($n=0, 1, 2, \ldots$) for a real G ($\theta=0$). But the reflection coefficient is always unity at $B/L=0.5n$ ($n=0, 1, 2, \ldots$). These can also be clearly observed in Fig. 5a. It is noted that the transmission coefficient for $d/h=1.0$ is always zero and that is not plotted in Fig. 5b. For the present partially immersed breakwater, the reflection coefficient still oscillates between its local maximum and minimum with the increasing value of B/L, as shown in Fig. 5a. The same phenomenon can also be observed for the transmission coefficient in Fig. 5b. Moreover, it can be seen from Fig. 5 that with the increasing value of d/h the transmission coefficient decreases monotonously. But the variation of the reflection coefficient with the increasing value of d/h is relevant to B/L. That is to say, increasing d/h does not necessarily lead to a larger reflection coefficient. This has also been observed in the experiments of Brossard et al. (2003). We note from Fig. 5 that with the increasing value of B/L, the reflection and transmission coefficients for a fixed d/h may simultaneously decrease or increase. This is due to the fact that the perforated front wall can dissipate the incident wave energy and that the energy-loss coefficient oscillates with the increasing value of B/L. But for a partially immersed impermeable wall, the energy-loss coefficient is always zero in the context of linear potential theory. Then the decrease of wave reflection must lead to the increase of wave transmission, as shown in Fig. 2. By comparing different curves in Fig. 5, a moderate value of $d/h=0.5$ with appropriate B/L should be suitable for obtaining lower reflection and transmission coefficients simultaneously.

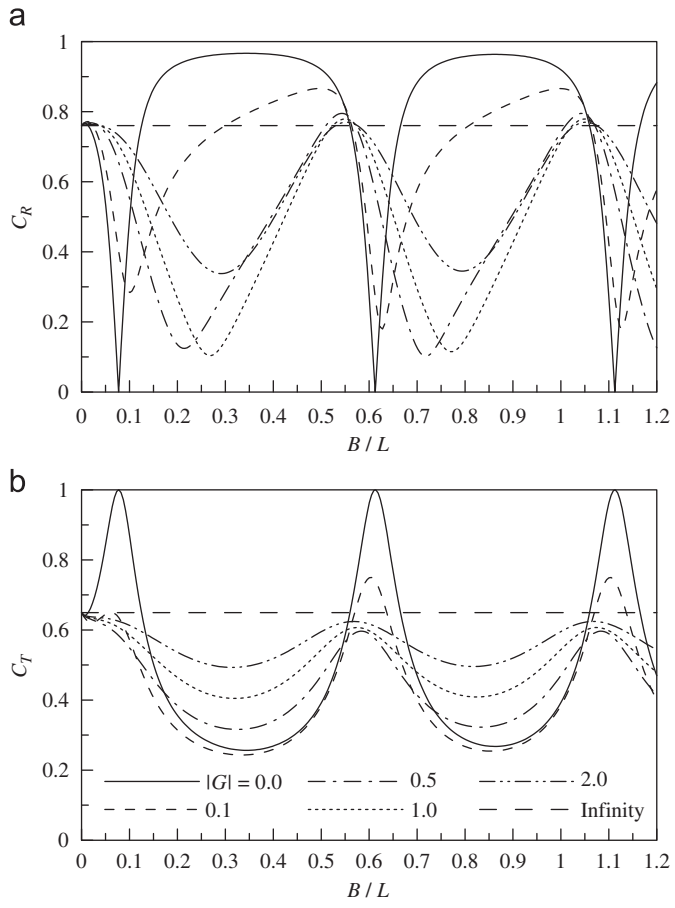

Fig. 6. Effects of $|G|$ on C_R and C_T: $k_0h=1.6$, $d/h=0.5$ and $G=|G|e^{0i}$. (a) C_R; (b) C_T.

Fig. 6 shows the effects of $|G|$ of the perforated front wall on C_R and C_T at $k_0h=1.6$, $d/h=0.5$ and $G=|G|e^{0i}$. The solid line in Fig. 6 denotes double partially immersed impermeable walls. For this structure, the energy-loss coefficient is zero ($C_L=0$). Thus the variation of C_R versus B/L is just the opposite to that of C_T versus B/L, as shown in Fig. 6. In other words, the double impermeable walls cannot provide effective shelter (lower transmission coefficient) concurrent with lower reflection coefficient. It is also noted from Fig. 6 that at some special values of B/L, the full transmission may occur for double impermeable walls (also see McIver, 1985; Das et al., 1997), i.e., the breakwater is totally ineffective. When the front wall is perforated, some of the incident wave energy can be dissipated by the wall. Following Yu and Chwang (1994), the energy dissipation is mainly determined by the porous effect parameter G, and a moderate G leads to maximum energy dissipation. Thus for different G, the variations of C_R and C_T with the increasing value of B/L are rather different as shown in Fig. 6. For $|G|=0.1$, the variation of C_R versus B/L is almost the opposite to that of C_T versus B/L. This is similar to the double impermeable walls. For $|G|\geq 0.5$, the variations of C_R and C_T with B/L are somewhat similar, although the location of local minimum C_T moves a bit to larger B/L in comparison with that of C_R. This makes it possible for the concurrence of lower reflection and transmission coefficients. When $|G|$ tends toward infinity, the front wall vanishes and then the values of C_R and C_T are both constants for different B/L. By carefully examining different curves in Fig. 6, it is evident that a moderate value of $|G|=0.5$–1.0 should be suitable for obtaining lower reflection and transmission coefficients simultaneously. The experimental studies of Li et al. (2002, 2006) showed that for $k_0h=1.30$–1.72 and $\varepsilon=20\%$, the value of $|G|$ is usually about 0.7–0.53 and that the argument of G is small. Therefore, a porosity of 20% may be appropriate for the breakwater. This has also been adopted in the major tests of Cox et al. (1998).

The effects of the dimensionless incident wave number k_0h (also is equivalent to the relative water depth h/L) on C_R and C_T are shown in Fig. 7 at $d/h=0.5$, $\delta/h=0.02$, $\varepsilon=20\%$, $f=9.0$ and $s=1.0$. Here the value of G is calculated by Eq. (13), since G may vary with the wave number k_0h. By comparing Fig. 7 with Fig. 5, it is found that increasing the incident wave number or increasing the relative draft gives similar effect on the reflection and transmission coefficients. From Fig. 7a, it can be seen that with the increasing value of k_0h, the location of the local minimum C_R moves to the left (smaller B/L). From Fig. 7b, it is evident that with the increasing value of k_0h, the shelter ability of the breakwater increases. This is well known and has also been observed in the tests of Neelamani and Vedagiri (2002) for double partially immersed impermeable walls. By further examining Fig.7, it is satisfactory to found that for moderate relative water depth ($k_0h=1.6$–2.8), the reflection and transmission coefficients of the present breakwater are both below 0.5 at $B/L=0.15$–0.35. Especially for $k_0h=2.2$, the values of C_R and C_T are both below 0.3 at $B/L=0.14$–0.27. This should be attractive for practical engineering. It should be mentioned that when the relative water depth further increases ($k_0h\geq 2.8$), the present structure is still very effective. Our further numerical results indicate that for $k_0h\geq 2.8$, very small reflection and transmission coefficients can be obtained simultaneously by a moderate increase in the porosity of the front wall.

Fig. 8 shows the effects of the argument θ of the porous effect parameter G on C_R and C_T at $k_0h=1.6$, $d/h=0.5$ and $G=0.5e^{i\theta}$. In fact, the value of θ is usually small for thin perforated walls in

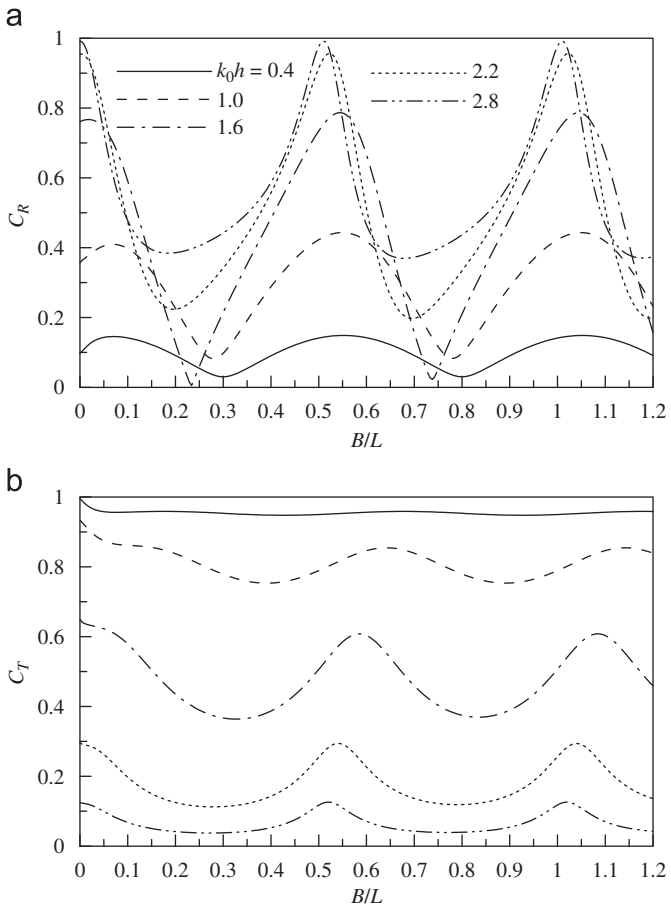

Fig. 7. Effects of k_0h on C_R and C_T: $d/h=0.5$, $\delta/h=0.02$, $\varepsilon=20\%$, $f=9.0$ and $s=1.0$. (a) C_R; (b) C_T.

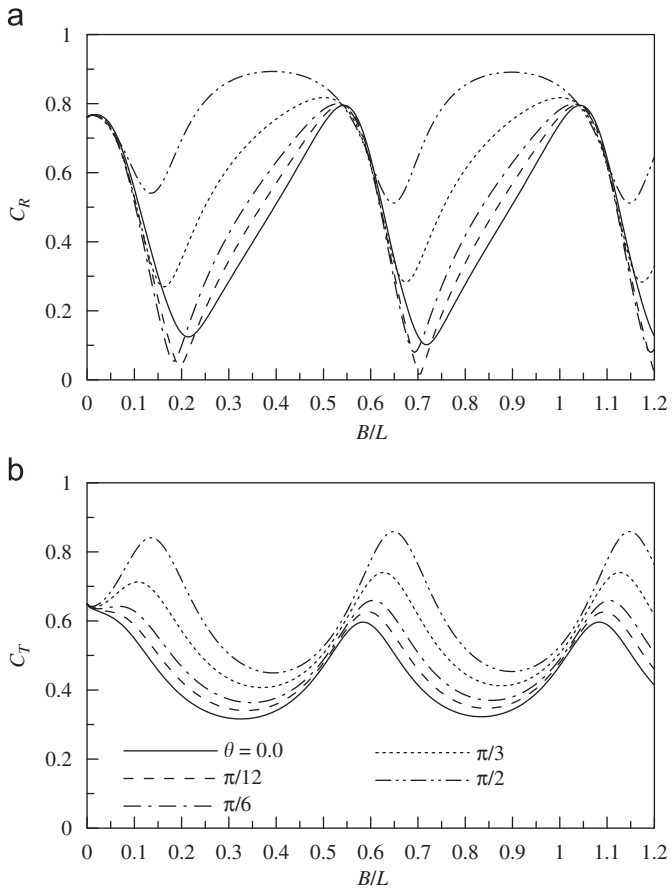

Fig. 8. Effects of θ on C_R and C_T: $k_0h=1.6$, $d/h=0.5$ and $G=0.5e^{i\theta}$. (a) C_R; (b) C_T.

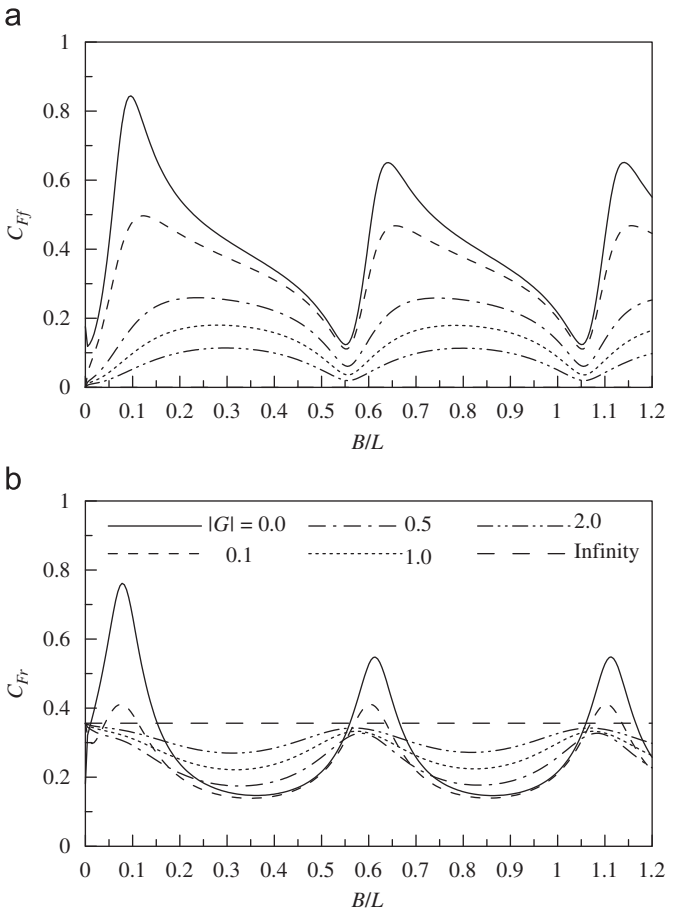

Fig. 9. Effects of $|G|$ on C_{Ff} and C_{Fr}: $k_0h=1.6$, $d/h=0.5$ and $G=|G|e^{0i}$. (a) C_R; (b) C_T.

practice (Li et al., 2002; Li et al., 2006). It even may be treated as zero (Cho and Kim, 2000). But the variations of C_R and C_T with the increasing value of θ (from 0 to $\pi/2$) are examined for interest. It can be seen from Fig. 8a that the location of local minimum reflection coefficient moves to the left with the increasing value of θ. But a contrary result can be observed for the transmission coefficient in Fig. 8b. Here the interesting case is $\theta=\pi/2$. At this time, the porous effect parameter G is a pure imaginary and then the energy-loss coefficient C_L equals zero. Thus the variation of C_R versus B/L is just the opposite to that of C_T versus B/L, as shown in Fig. 8. Now the existence of the perforated front wall only changes the phase of wave motion.

Finally, the wave force acting on each wall is shown in Fig. 9. The calculating conditions are $k_0h=1.6$, $d/h=0.5$ and $G=|G|e^{0i}$, which are the same as for Fig. 6. It can be seen from Fig. 9a that the dimensionless wave force C_{Ff} on the front wall decreases significantly with the increasing value of $|G|$. This is very helpful to enhancing the stability of the wall. When $|G|$ tends toward infinity, the value of C_{Ff} attains zero and is not plotted in Fig. 9a. By comparing Fig. 9a with Fig. 6a, it is found that the variation of C_{Ff} versus B/L is almost the opposite to that of C_R versus B/L. This has also been observed by Yip and Chwang (2000) for a bottom-standing Jarlan-type breakwater with a horizontal impermeable plate. The reason is that for minimum C_R the surface elevation difference between the two sides of the front wall is very large. Thus C_{Ff} is large. But for maximum C_R, the surface elevation difference is very small. Hence C_{Ff} is small. From Fig. 9b, it can be seen that for $|G|=0$ the maximum C_{Fr} on the rear wall is rather large. But when perforating the front wall, the value of maximum C_{Fr} decreases significantly. In addition, it is interesting to find that the variation of C_{Fr} versus B/L is the same as that of C_T versus B/L by comparing Fig. 9b with Fig. 6b. This indicates that the variation of the surface elevation difference between the two sides of the rear wall should be consistent with C_T. From Fig. 9, it can also be seen that the magnitudes of wave forces acting on the two walls are close and small at $|G|=0.5$–1.0. At this time, the wave absorbing ability of the breakwater is also satisfactory as shown in Fig. 6.

5. Conclusions

On the basis of the eigenfunction expansion method and a least square approach, the present study has developed an analytical solution to assess the hydrodynamic performance of a wave absorbing double curtain-wall breakwater. The new developed solution has been validated by comparing the numerical results for several limiting cases with previous predictions. The present method has also been validated by comparing the numerical results with previous experimental data. Thus the present method may be used for practical engineering at a preliminary design stage.

Numerical examples show that the reflection coefficient C_R and the transmission coefficient C_T of the breakwater are mainly determined by the relative wave chamber width B/L, the relative draft d/h, the dimensionless incident wave number k_0h and the geometrical porosity ε of the front wall (denoted by G). It seems that the effects of these four parameters are all significant. In addition, increasing d/h or k_0h gives similar effect to C_R and C_T. The numerical results also show that with suitable values of $d/h=0.5$, $\varepsilon=20\%$ and $B/L=0.15$–0.35, the values of C_R and C_T can be simultaneously controlled below 0.5, even 0.3, at $k_0h=1.6$–2.8.

The corresponding magnitudes of dimensionless wave forces acting on the two walls are also small and close. Moreover, the variation of C_{Ff} versus B/L is almost the opposite to that of C_R versus B/L. But the variation of C_{Fr} versus B/L is the same as that of C_T versus B/L.

Acknowledgments

This work was financially sponsored by the Natural Science Foundation of China (50909086; 50921001), the Specialized Research Fund for the Doctoral Program of Higher Education (200804231006) and the Natural Science Foundation of Shandong Province (Q2008F01).

References

Abul-Azm, A.G., 1993. Wave diffraction through submerged breakwaters. Journal of Waterway, Port, Coastal, and Ocean Engineering, ASCE 119 (6), 587–605.
Bennett, G.S., McIver, P., Smallman, J.V., 1992. A mathematical model of a slotted wavescreen breakwater. Coastal Engineering 18, 231–249.
Brossard, J., Jarno-Druaux, A., Marin, F., Tabet-Aoul, E.H., 2003. Fixed absorbing semi-immersed breakwater. Coastal Engineering 49, 25–41.
Chen, K.H., Chen, J.T., Lin, S.Y., Lee, Y.T., 2004. Dual Boundary element analysis of normal incident wave passing a thin submerged breakwater with rigid, absorbing, and permeable boundaries. Journal of Waterway, Port, Coastal, and Ocean Engineering, ASCE 130 (4), 179–190.
Chen, X.F., Li, Y.C., Kong, L., 2009. The calculation of wave forces on perforated breakwaters. In: Proceeding of the Fifth International Conference on Asia and Pacific Coasts (APAC 2009), Singapore, vol. 3, pp. 304–311.
Cho, I.H., Kim, M.H., 2000. Interactions of horizontal porous flexible membrane with waves. Journal of Waterway, Port, Coastal, and Ocean Engineering, ASCE 126 (5), 245–253.
Chwang, A.T., 1983. A porous-wavemaker theory. Journal of Fluid Mechanics 132, 395–406.
Chwang, A.T., Dong, Z., 1984. Wave-trapping due to a porous plate. In: Proceedings of the 15th Symposium on Naval Hydrodynamics, Session 6, Hamburg, pp. 32–42.
Cox, R.J., Horton, P.R., Bettington, S.H., 1998. Double walled, low reflection wave barriers. In: Proceedings of the 26th Coastal Engineering Conference, ASCE, Copenhagen, Denmark, pp. 2221–2234.
Dalrymple, R.A., Martin, P.A., 1990. Wave diffraction through offshore breakwaters. Journal of Waterway, Port, Coastal, and Ocean Engineering, ASCE 116 (6), 727–741.
Das, P., Dolai, D.P., Mandal, B.N., 1997. Oblique wave diffraction by parallel thin vertical barriers with gaps. Journal of Waterway, Port, Coastal, and Ocean Engineering, ASCE 123 (4), 163–171.
Fugazza, M., Natale, L., 1992. Hydraulic design of perforated breakwaters. Journal of Waterway, Port, Coastal, and Ocean Engineering, ASCE 118 (1), 1–14.
Günaydın, K., Kabdaşlı, M.S., 2007. Investigation of Π-type breakwaters performance under regular and irregular waves. Ocean Engineering 34, 1028–1043.
Huang, Z.H., 2006. A method to study interactions between narrow-banded random waves and multi-chamber perforated structures. Acta Mechanica Sinica 22 (4), 285–292.
Huang, Z.H., 2007. Reflection and transmission of regular waves at a surface-pitching slotted barrier. Applied Mathematics and Mechanics 28 (9), 1153–1162.
Isaacson, M., Baldwin, J., Premasiri, S., Yang, G., 1999. Wave interactions with double slotted barriers. Applied Ocean Research 21, 81–91.
Isaacson, M., Premasiri, S., Yang, G., 1998. Wave interactions with vertical slotted barrier. Journal of Waterway, Port, Coastal, and Ocean Engineering, ASCE 124 (3), 118–126.
Jarlan, G.E., 1961. A perforated vertical wall breakwater. The Dock and Harbour Authority 41 (486), 394–398.
Ketabdari, M.J., Varjavand, I., 2008. Reflected energy spectrum from slotted breakwaters due to irregular waves. Journal of Coastal Research 24 (6), 1529–1535.
Kriebel, D.L., Bollmann, C.A., 1996. An assessment of power transmission theory for vertical wave barrier. In: Proceeding of the 25th Coastal Engineering Conference, ASCE, Orlando, Florida, pp. 2470–2483.
Lee, M.M., Chwang, A.T., 2000. Scattering and radiation of water waves by permeable barriers. Physics of Fluids 12 (1), 54–65.
Lee, W.K., Lo, E.Y.M., 2002. Surface-penetrating flexible membrane wave barriers of finite draft. Ocean Engineering 29, 1781–1804.
Li, Y.C., 2007. Interaction between waves and perforated-caisson breakwaters. In: Proceedings of the Asian and Pacific Coasts 2007, Nanjing, China, pp. 1–16.
Li, Y.C., Liu, H.J., Teng, B., Sun, D.P., 2002. Reflection of oblique incident waves by breakwaters with partially-perforated wall. China Ocean Engineering 16 (3), 329–342.
Li, Y.C., Liu, Y., Teng, B., 2006. Porous effect parameter of thin permeable plates. Coastal Engineering Journal 48 (4), 309–336.
Liu, P.L.F., Abbaspour, M., 1982. Wave scattering by a rigid thin barrier. Journal of Waterway, Port, Coastal, and Ocean Engineering, ASCE 108 (4), 479–491.
Liu, Y., Li, Y.C., Teng, B., 2007. Wave interaction with a new type perforated breakwater. Acta Mechanica Sinica 23, 351–358.
Liu, Y., Li, Y.C., Teng, B., Jiang, J.J., Ma, B.L., 2008. Total horizontal and vertical forces of irregular waves on partially perforated caisson breakwaters. Coastal Engineering 55, 537–552.
Losada, I.J., Losada, M.A., Roldán, A.J., 1992. Propagation of oblique incident waves past rigid vertical thin barriers. Applied Ocean Research 14, 191–199.
McIver, P., 1985. Scattering of water waves by two surface-piercing vertical barriers. IMA Journal of Applied Mathematics 35, 339–355.
Neelamani, S., Vedagiri, M., 2002. Wave interaction with partially immersed twin vertical barriers. Ocean Engineering 29, 215–238.
Porter, R., Evans, D.V., 1995. Complementary approximations to wave scattering by vertical barriers. Journal of Fluid Mechanics 294, 155–180.
Rageh, O.S., Koraim, A.S., Salem, T.N., 2009. Hydrodynamic efficiency of partially immersed caissons supported on piles. Ocean Engineering 36 (14), 1112–1118.
Reddy, M.S., Neelamani, S., 1992. Wave transmission and reflection characteristics of a partially immersed rigid vertical barrier. Ocean Engineering 19 (3), 313–325.
Sahoo, T., Lee, M.M., Chwang, A.T., 2000. Trapping and generation of waves by vertical porous structures. Journal of Engineering Mechanics, ASCE 126 (10), 1074–1082.
Sollitt, C.K., Cross, R.H., 1972. Wave transmission through permeable breakwaters. In: Proceedings of the 13th Coastal Engineering Conference, ASCE, Vancouver, pp. 1827–1846.
Suh, K.D., Park, J.K., Park, W.S., 2006a. Wave reflection from partially perforated-wall caisson breakwater. Ocean Engineering 33, 264–280.
Suh, K.D., Shin, S., Cox, D.T., 2006b. Hydrodynamic characteristics of pile-supported vertical wall breakwaters. Journal of Waterway, Port, Coastal, and Ocean Engineering, ASCE 132 (2), 83–96.
Tabet-Aoul, E.H., Lambert, E., 2003. Tentative new formula for maximum horizontal wave forces acting on perforated caisson. Journal of Waterway, Port, Coastal, and Ocean Engineering, ASCE 129 (1), 34–40.
Takahashi, S., 1996. Design of vertical breakwaters. Reference Document N34. Port and Harbour Research Institute, Japan.
Tanimoto, K., Yoshimoto, Y., 1982. Theoretical and experimental study of reflection coefficient for wave dissipating caisson with a permeable front wall. Report of the Port and Harbour Research Institute 21 (3), 44–77 (in Japanese, with English abstract).
Teng, B., Zhang, X.T., Ning, D.Z., 2004. Interaction of oblique waves with infinite number of perforated caissons. Ocean Engineering 31, 615–632.
Twu, S.W., Lin, D.T., 1991. On a highly effective wave absorber. Coastal Engineering 15, 389–405.
Ursell, F., 1947. The effect of a fixed vertical barrier on surface waves in deep water. Proceedings of the Cambridge Philosophical Society 43 (3), 374–382.
Wiegel, R.L., 1960. Transmission of waves past a rigid vertical barriers. Journal of Waterways and Harbour Division, ASCE 86 (1), 1–12.
Williams, A.N., Mansour, A.E.M., Lee, H.S., 2000. Simplified analytical solutions for wave interaction with absorbing-type caisson breakwaters. Ocean Engineering 27, 1231–1248.
Yip, T.L., Chwang, A.T., 2000. Perforated wall breakwater with internal horizontal plate. Journal of Engineering Mechanics, ASCE 126 (5), 533–538.
Yu, X.P., 1995. Diffraction of water waves by porous breakwaters. Journal of Waterway, Port, Coastal, and Ocean Engineering, ASCE 121 (6), 275–282.
Yu, X.P., Chwang, A.T., 1994. Water waves above submerged porous plate. Journal of Engineering Mechanics, ASCE 120 (6), 1270–1282.
Zhu, S.T., Chwang, A.T., 2001. Investigations on the reflection behaviour of a slotted seawall. Coastal Engineering 43, 93–104.